GCEP Progress Report

"Collaborative Research on Carbon Sequestration in Saline Aquifers in China"

Investigators

Dongxiao Zhang, Professor, Hydrogeology and Petroleum Engineering; Kristian Jessen, Assistant Professor, Peteoleum Engineering; Hamid Jahangiri, Dalad Nattwongasem, Graduate Researcher, University of Southern California;

Bin Gong, Research Scientist, Energy & Resources Engineering; Qingdong Cai, Associate Professor, Mechanics; Yi Zheng, Research Scientist, Energy & Resources Engineering; Haibin Chang, Xuan Liu, Ming Lei, Zhijie Wei, Xiang Li, Yongbin Zhang, Graduate Researchers, Peking University;

Yilian Li, Professor, Geochemistry; Yanxin Wang, Hydrogeology and Geochemistry; Jianmei Cheng, Hydrogeology; Wei Zhang, Ling Jiang, Gengbiao Qiu, Qi Fang, Yibing Ke, Peng Cheng, Sanxi Peng, Ronghua Wu, Jianxiong Dong, Anne Nyatichi Omambia, and Kabera Telesphore, Graduate Researchers, China University of Geosciences.

Abstract

This work represents the international collaborative efforts by researchers from Peking University, China University of Geosciences at Wuhan, and University of Southern California to address fundamental issues associated with large-scale sequestration of CO_2 in saline formations with emphasis on developing the potential for CO_2 sequestration projects in China.

The collaborative research aims to address 1)Salt precipitation and pressure buildup during CO_2 injection; 2)Validation of the accuracy of numerical simulations based on co-current relative permeability functions; and3) Enhancement of the performance of the existed reactive transport simulator, and extension of modeling Enhanced Coal Bed Methane process.

In the first part, two methods were tried to relieve salt precipitation and pressure buildup during CO_2 injection. Pre-flush with fresh water before CO_2 injection can obviously alleviate the pressure buildup induced by halite precipitation around the injection well. In addition, it could lower the salinity of the aquifers and increase the solubility of CO_2, with the benefit of reducing the leakage risk. Pumping saline water out of the target formation while injecting CO_2 could reduce the pressure buildup both in the near-well region and the formation as whole. Increase in the water production rate leads to further decrease in pressure buildup, this phenomenon

was demonstrated by tripling the production where the pressure decreased about 15 bars. The introduction of two wells (left side and right side of the production well) increases the horizontal migration of the CO_2 but contributes a little to the amount of CO_2 dissolved.

In the second part, four-electrode resistivity measurements were used to monitor the migration of the non-wetting phase by relating the resistivity index (RI) to the brine saturation. The observations are compared with numerical calculations to demonstrate that co-current relative permeability functions, that were measured directly, are inadequate to reproduce the experimental observations.

In the third part, we present our progress on stabilizing the geochemical simulator and the implementation of Enhanced Coal Bed Methane to a General Propose Reservoir Simulator Chemical Reaction Module. The former section of this part presents our progress on designing a general scheme to eliminate equilibrium reaction rates for GPRS chemical reaction simulator. Then we introduce the procedure of extending chemical simulator to model CBM/ECBM process. The idea is based on the fact that gas sorption is solely a kinetic chemical reaction whose reaction rate is correlated with gas pressure or other environmental parameters. Differ from the common CBM/ECBM simulators, geochemical approach has a better handle of complex adsorption model, which leave us a wider space to enhance the current Langmuir type reaction sorption model. Cases are carried out to validate the approach.

Introduction

Solutions to salt precipitation and pressure buildup during CO_2 injection into saline aquifers in Jianghan Basin

As pressure buildup due to CO_2 injection in saline aquifers, especially under the context of high salinity, can be the most limiting factors affecting the injectivity, strategies of relieving pressure are urgently needed to be considered. The aim of the present work is to investigate the solutions of reducing salt precipitation and pressure buildup during CO_2 injection to saline aquifers. Two solutions are introduced. One refers to pre-flushing the saline water with the fresh water before CO_2 injection; the other refers to pumping out saline formation water and injecting CO_2 simultaneously to control pressure buildup.

Dynamics of Plume Migration in Counter-Current Flows

A reduction in the relative permeability of both phases is required to improve the agreement between experimental observations and numerical calculations. Numerical calculations based on co-current input data predicts a much faster migration of iC8 to the top of the column than what is observed in the segregation experiments. Our findings demonstrate that the prevailing flow regime affects the phase mobilities, in part because of the viscous coupling, and must therefore be

considered in displacement processes where counter-current flow may occur, such as during injection/storage of CO_2 in saline aquifers.

Enhancement of Geochemical Simulator and the application in ECBM

In this work, we first present the supplement of GPRS geochemical simulator. The key issue we focus on is to design a general scheme to eliminate fast thermodynamic equilibrium reaction rates from the species conservation equations. The Equilibrium Rate Annihilation (ERA) matrix method and Decomposing Method are introduced. An illustration of ECBM implemented GPRS chemical simulator is also presented in the later section. The validations of our model are performed by comparing the results with commercial software which is widely used in ECBM. It should be noted that the sorption model we used at present is also the Langmuir type sorption model. Reaction occurs in the aqueous phase is not included in current work. More sophisticated models are under investigation.

Background

Solutions to salt precipitation and pressure buildup during CO_2 injection into saline aquifers in Jianghan Basin

Two solutions to salt precipitation and pressure buildup were tried in the present work. For using pre-flush with water before CO_2 injection, a 2D radially symmetric model was used to represent a CO_2 storage site in the Qianjiang depression area (Figure 1). The storage formation into which CO_2 is injected is 120 m thick and located at a depth of about 1380 m below the ground surface. The storage formation is bounded at the top by a sealing layer of 30 m, followed by a sequence of aquifers with various thicknesses and sealing layers with various thicknesses. The model domain includes four aquifers and five aquitards. The lateral extent boundary at 200 km corresponds to a footprint area of about 125,664 km^2. The large lateral extent was chosen in order to ensure that the boundary condition would have minimal effect on the simulation results. The sand permeability and porosity of the target formation is 9×10^{-13} m^2 and 0.16, respectively. For the sealing layer, the permeability and porosity of the mudstones is 9×10^{-17} $m^2$and 0.10. Carbon dioxide is injected into a zone where lies in the depth of about 1512m at the rate of 50 kg/s. The simulation time runs cover a time period of two years injection. For base case, we first inject water for 2 months, and then inject CO_2 for 2 years.

For pumping out saline formation water while injecting CO_2,2D (XZ) model is used to simulate the storage process around an injection well in this work, with a permeability of $77.6*10^{-15}$ m^2, a porosity of 15.4 % [16] and a net aquifer of 110 m with Caprock as well as Baserock of 20 m each. The aquifer temperature is 89^{o}C corresponding to temperature in Jianghan basin at the depth of about 2200 m [17]. Relative permeability was modeled using the van Genuchten- Mualem model and the Corey's function was used to get relative permeability for free CO_2 phase. A vertical

saline formation water well of 30 m thickness from the bottom of aquifer is placed at 9.5 km (left and right sides of the CO_2 injection well) from the CO_2 injection well (Figure 2) whereas for carbon dioxide injection well was placed in the middle of the aquifer and the injection height is similar to the saline formation water well height, 30 m for both.

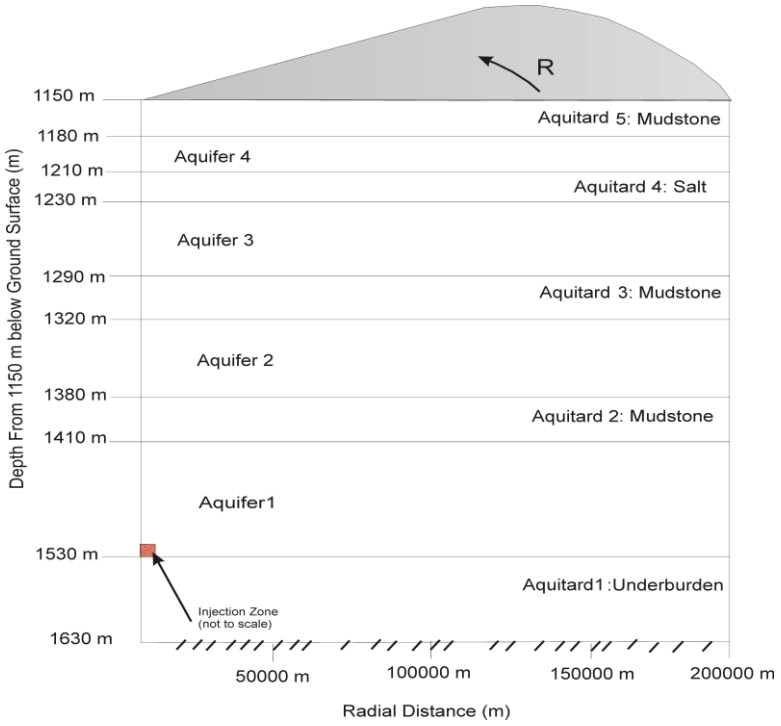

Figure 1: Radial symmetric model domain with deep brine formation in Jianghan Basin.

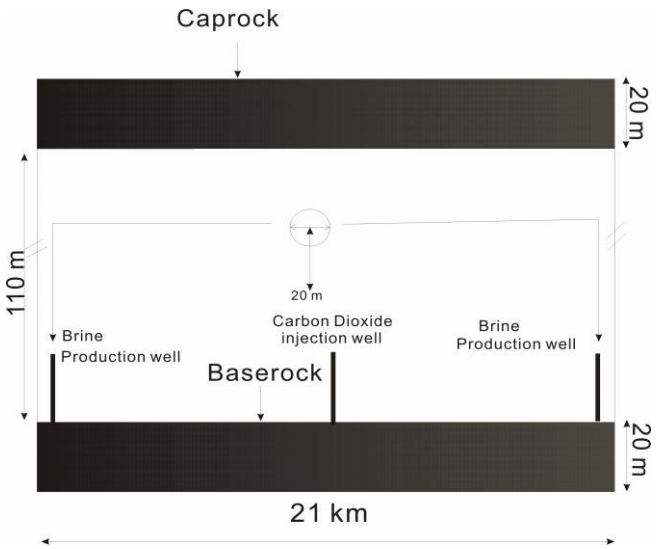

Figure 2: Schematic diagram of placement of injection and production wells

Dynamics of Plume Migration in Counter-Current Flows

The porous media use in this work consists of a borosilicate glass column with adjustable plungers. The glass column has an inner diameter of 50 mm and a height of 500 mm. Stainless steel frits (type 316) with an average pore size of 10 μm were attached to the end of each plunger. The frits were used as current electrodes and to create a uniform flow distribution of injected fluids. A hole was drilled through each plunger and an electrical wire was inserted to connect the metal frits to a power source without disturbing the flow. The glass column was further modified by drilling holes along the length to insert the potential electrodes. In each selected interval, three holes were drilled on the perimeter of the column with a spacing of 120 degrees. A total of 36 holes were drilled along the glass column to establish a total of 11 sections. The electrodes were placed in contact with the beads through the holes along the column and carefully sealed with epoxy to prevent leakage. At each level along the column, the 3 wires were connected together and used as the voltage electrodes.

To represent and study the migration of a supercritical CO_2 plume in a saline aquifer, we conducted a series of segregation experiments at low-pressure using the synthetic porous material and analog fluids. We used BT13 (170 Mesh) glass beads with an average particle diameter of 88 μm to represent the porous media while the immiscible two-phase brine/iso-octane (iC8) fluid system was used to represent brine/supercritical CO_2 at reservoir conditions. Brine was prepared from deionized water and NaCl with a concentration of 20,000 ppm resulting in a density of 1013 kg/m3 at 70°F while the non-wetting phase (iC8) has a density of 692 kg/m3 at 70°F. To visualize the propagation of iC8 in the column we used an oil soluble dye (Sudan Red 7B). The viscosity of brine and iC8 are 1.0 and 0.48 mPa.s, respectively, as reported by Cinar et al. (2006). Pendant drop measurement was performed to determine the interfacial tension of the brine/iC8 system and a value of 47.3 mN/m was observed from repeated measurements.

The porosity and permeability of the packed column were measured to 38.6% and 4.8 Darcy, respectively. At fully saturated conditions, the porosity at each section of the column was calculated from the resistance and found to be in good agreement with the overall porosity.

Relative permeability functions for primary drainage and imbibition processes were measured from steady-state flow experiments. Figure 3 reports the relative permeability measurements and a Corey-type representation for both drainage and imbibition processes.

Capillary pressure functions were adopted from Dawe et al. (1992), who measured capillary pressure for drainage and imbibition processes in glass bead packs. As their measurements were performed for different glass bead sizes and fluid systems, their capillary pressure observations were initially scaled using Leverett J-scaling (Leverett, 1941).

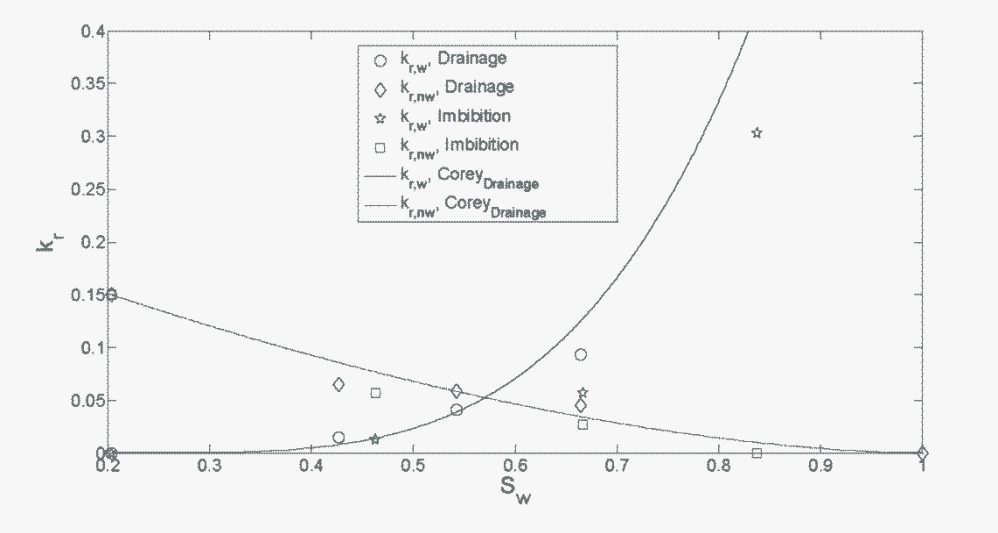

Figure 3: Steady-state relative permeability functions for drainage and imbibition processes

The primary drainage and imbibition capillary pressures corresponding to the glass bead used in our segregation experiments were constructed from the J-functions extracted from Dawe et al. (1992): van Genuchten (1980) capillary pressure functions were used to smooth the capillary pressure data for both drainage and imbibition processes. To match the irreducible wetting phase saturation and maximum trapped non-wetting saturation obtained from our steady-state relative permeability experiments, we re-normalized the phase saturations. In addition, the drainage capillary pressure was measured using the porous-plate technique. The capillary pressure function was subsequently re-scaled to fit the measured values.

In order to capture the dynamic changes in the electric potential across the individual sections of the column during segregation experiments, two data acquisition modules from National Instruments (NI-DAQ) were used to provide and acquire signals. A 0.5 V AC signal with frequency of 1 kHz was generated from the analogue channel of one NI-DAQ unit. A shunt resistor with a resistance of 2 kΩ was connected in series to the top of the packed column to prevent current overflow (and accelerated corrosion). The wires from the packed column were connected to the analogue input channels of the second NI-DAQ module. Both NI-DAQ modules were connected to a PC to control the units and to collect data. The potential difference across each section of the packed column and across the shunt resistor was continuously recorded using LabView software. Figure 4 shows a schematic diagram of the dynamic segregation experiment including connections to the source and acquisition systems. Once the column was fully saturated with brine, the resistivity of each section of the packed column was determined.

A Teledyne 260D syringe pump was used to inject iC8 at the top of the column at a rate below the critical velocity as calculated from the petro-physical properties

discussed earlier. The dyed iC8 was then injected into the column to create an initial non-wetting saturation distribution as uniform as possible. After the desired amount of iC8 was injected, the packed column was inverted and the segregation experiment initiated. The potential differences at each section of the packed column were continuously recorded allowing for subsequent calculation of the wetting phase saturation from the resistivity index.

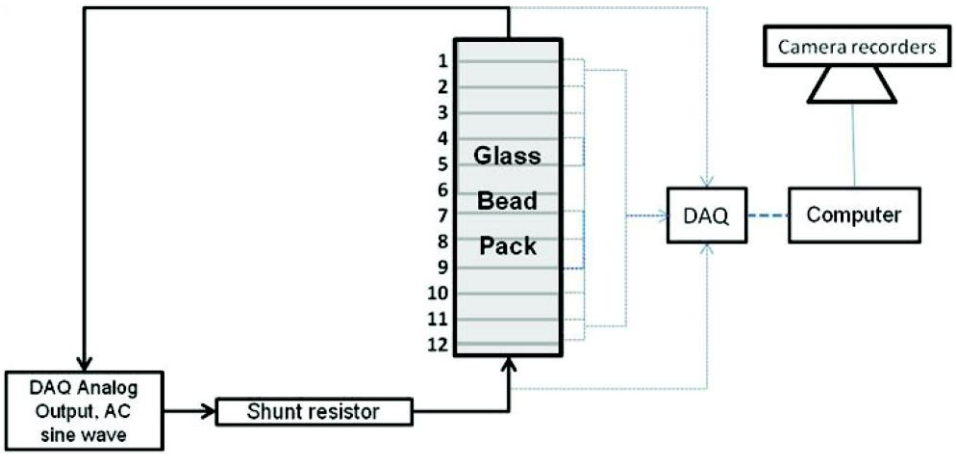

Figure 4: Schematic diagram of experimental setup for segregation experiment

To repeat the segregation experiment, two pore-volumes of isopropanol were injected to remove iC8 and brine from the column. Deionized water was subsequently used to flush the column and remove the isopropanol and finally, brine was loaded from the bottom to displace the deionized water.

Enhancement of Geochemical Simulator and the application in ECBM

Chemical reaction and transport in the subsurface occurs over a wide range of space and time scales. For a given amount of mass at a fix point and time, chemical reactions determine the partition of the components among different phases. The reactions can be typically divided into two classes: equilibrium reactions whose reaction rates are fast and reversible and the kinetic reactions with finite rates. As the rates of thermodynamic equilibrium reaction are fast and hard to be detected, a direct solution for the species mass balance equation is unpractical. Some strategies have been introduced to solve this problem. Among them there are Equilibrium Rate Annihilation (ERA) matrix method and Decomposing method. Meanwhile, these methods reduce the number of mass balance equations to be solved.

Previous version of GPRS geochemical simulator uses an element-balance approach to reduce the number of equations as well as eliminate fast reactions rates. The element can be but not limited to the concept of atoms in the sense of chemistry. This approach based on a simple relation that the reaction stoichiometric matrix

multiplied by the stoichiometric coefficients matrix is zero under the assumption of element balance. It can be shown as

$$\mathrm{E}_{n_e \times n_c} \mathrm{S}_{n_c \times n_r} = 0_{n_e \times n_r}$$

Where E and S are reaction stoichiometric matrix and component-element correlation matrix, respectively. It is straightforward to use component-element correlation matrix to derive ERA matrix. However, some researchers declare that it may lead to numerical solving problem when some member of elements is very low and the other is several orders of magnitude higher. Another ERA building strategy is adapted to the simulator which has been reported in the literature [35]. It assumes equilibrium reactions only exist in the aqueous phase. For aqueous part, the reactions and the corresponding stoichiometric matrix can be expressed as:

$$V = \begin{bmatrix} v_{1,1} & \cdots & v_{1,R_{aq}} \\ \vdots & \vdots & \vdots \\ v_{n_{ca},1} & \cdots & v_{n_{ca},R_{aq}} \end{bmatrix}_{n_{ca} \times R_{aq}}$$

$\mathrm{n_{ca}}$ is the number of aqueous species and $\mathrm{R_{aq}}$ is the number of aqueous reactions.

The canonical stoichiometric matrix has the following form:

$$V_c = \begin{bmatrix} V_{p \times R_{aq}} \\ I_{R_{aq} \times R_{aq}} \end{bmatrix}_{n_{ca} \times R_{aq}}$$

I is the identity matrix. The subscript p denotes the number of primary species or components. To eliminate equilibrium rates in the mass balance equations, ERA matrix must be non-singular and satisfies

$$EV_c = 0$$

Then the ERA matrix can be

$$E = [I_{p \times p}, -V_{p \times R_{aq}}]$$

Dissolution–precipitation only involves one mineral species normally. Therefore the stoichiometric coefficient is all zeros except for the corresponding mineral species mass balance function. The kinetic rate term that was included in aqueous species mass balance don't have to be eliminated. Then extended ERA matrix for the full system can be expressed as

$$\begin{array}{|c:c|} \hline ERA_{p\times n_{ca}} & U_{R_p\times R_{\min}} \\ \hdashline 0_{R_{\min}\times n_{ca}} & I_{R_{\min}\times R_{\min}} \\ \hline \end{array}$$

The matrix U can be any form only if it can keep the extended ERA matrix invertible. A validation is carried out by comparing our results with GEM, which also use the canonical matrix strategy. The case is a simpleCO_2mineralizationin aqueous. It involves four reactions listed below: three intra-aqueous chemical-equilibrium reactions and the mineral dissolution reaction. Stoichiometric matrix for aqueous part is shown in table 1. The ideal activity model is used for both simulators. Water vaporization is activated.

$$OH^- + H^+ = H_2O$$

$$CO_{2(aq)} + H2O = H^+ + HCO_3^-$$

$$H^+ + CO_3^{2-} = HCO_3^-$$

$$CaCO_{3(s)} + H^+ = Ca^{2+} + HCO_3^-$$

Table 1: Stoichiometric matrix for aqueous part

Species / Reaction	CO_2(aq)	H2O	H+	Ca++	OH-	HCO3-	CO3--
R1	0	1	-1	0	-1	0	0
R2	-1	-1	1	0	0	1	0
R3	0	0	-1	0	0	1	-1

The two methods mentioned above both aim to eliminate fast reactions rate in the species mass balance equations. ERA matrix is employed on the purpose. Decomposition Method is another option. The reactions can be written as a set of ODEs for each species. The main idea of the decomposition method is though gauss elimination to reduce the reactions into three subsets of equations: mass conservation equations, infinite rate equation that can be represented by equilibrium equation and finite rate of kinetic equation. The detail of the this method can be found in the paper reported by Fang, Y.(2003).

Although ERA matrix method and decomposition method are different approach, they are consistent in principle. The optimal method is chosen according to the problem and variable set.

CO_2 storage in coal seam is presently also an appealing way for reducing greenhouse gas emissions as well as a significant methane enhancement by experiments and field test. Differ from the conventional gas which is trapped in the pore space, the majority of gas in the CBM reservoir is stored in the coal matrix by sorption. The sorption effect makes CBM reservoir a vast potential volume for geological sequestration. CBM water also plays an important role in CO_2 flooding. In some places where the aqueous phase has high salinity contents, the solution of CO_2 is significantly impacted. It requires a coupled geochemical tool to model the process. Although there are a number of geochemical simulators are available at present, most of them are used for contamination and water resource issues. A coupled CBM/ECBM geochemical tool has been undertaken by some groups. One reported study comes from the Issued by Sandia National Laboratories, which modify the exiting geochemical simulator TOUGH2 on this purpose. Unfortunately no satisfying results are derived. Another group worth to mention is the Stanford University Petroleum Research Institute (SUPRI-B). A fully implicit transport and reactive model is implemented within the General Purpose Reservoir Simulator (GPRS). The modular object–oriented design facilitates he extension of GPRS chemical simulator to model ECBM process.

The main idea we implement the CBM/ECBM model is based on the similarity between of adsorption process of surface reaction and ECBM. Adsorption is the process by which fluid constituents adhere to a solid surface (i.e., the coal, in this case). To illustrate it, a basic knowledge of CBM adsorption process is necessary. The typical adsorption model we use is Langmuir isotherm, which is also available by most commercial software. To start with, we propose a single component, two-parameter Langmuir model of the following form

$$C(p_g) = \frac{V_L p_g}{(P_L + p_g)}$$

Where V_L is the maximum amount of gas that can be absorbed, and P_L is a characteristic pressure. Both V_L and P_L are determined from laboratory adsorption isotherm measurements. Under the assumption of local phase equilibrium between the entire domains, the adsorbed concentration on the surface of the coal is solely the function of pressure. Hence the pressure determines the storage capacity for coal seams. The initial concentration of methane is also calculated by means of this method.

For the prediction of mixed gas adsorption, convenient method is to extend the pure component Langmuir model to a multicomponent type. Then the adsorption capacity is function of pressure and composition. For each component in a system of $N_c$absorbablecomponent, the extended Langmuir model is yield to be

$$C_i = \frac{V_{L_i} p_i / P_{Li}}{(1+\sum_{j=1}^{N_c} p_j / P_{Lj})}$$

Where p_i is the partial pressure for the corresponding component and can be defined as

$$p_i = p_g y_{ig}$$

Langmuir parameters for pure component isotherms are also used. Diffusion of gas between the two media (cleat and matrix) is traditionally modeled as a Fickian process which is given by

$$F_g = \chi D_{ci} (C_{si} - C(p_i))$$

Where the diffusivity χ can be written as

$$\chi = V\sigma$$

The parameter V and σ are bulk volume and shape factor respectively.σ is the factor account for the interface area per unit volume. Commonly, the diffusion coefficient and the shape factor are combined to be diffusion time as below, which is easier to obtain in the lab

$$\tau = \frac{1}{D_{ci}\sigma}$$

Then the production rate from the adsorbed state to the cleat can be written as

$$q_i = \frac{V}{\tau}(C_{si} - C(p_i))$$

For a chemical reaction simulator, the adsorption process for each component can be represented by the following expression in a system of $N_c$absorbablecomponents.

$$M_i(g) \leftrightarrow M_i(a)$$

Where M_i(g) and M_i(a) are symbols of component i in the gas phase and in the adsorbed phase. The kinetic reaction rate $r_i$for unit coal volume is defined as

$$r_i = \frac{1}{\tau}(C_{si} - C(p_i))$$

A complete ODE form of this solid kinetic reaction is

$$-\frac{dC_{si}}{dt} = r_i$$

Due to the similarity between the present problem and the reaction module already implemented in GPRS, we only need to provide the derivatives of the reaction term with respect to the unknown variables.

The implemented chemical reaction module inherits the former compositional parts. Phase behavior is represented by Peng-Robinson Equation of State (EOS) model. The following relation can be yield for each component at phase equilibrium

$$f_i^{p1} - f_i^{p2} = 0$$

To form a complete system, many constrain equations are needed, which include the molar fraction constrains

$$\sum_i X_{i,j} = 1$$

And saturation constrains

$$\sum_j S_j = 1$$

Then a fully equation system is well defined. For a primary CBM recovery problem, the species in the system are: CH4 (g), CH4 (l), H2O (g), H2O (l), CH4(s), where the script g, l, s indicates gas, liquid and solid phase. If we choose the element based ERA, the elements are: CH4, H2O. The component-element correlation matrix and reaction coefficient are tabled as table2 and table3.

Table 2: Component-element correlation matrix

	CH4	H2O	CH4s
CH4	1	0	1
H2O	0	1	0

Table 3: Reaction coefficient matrix

	CH4(g)	H2O(g)	CH4(l)	H2O(l)	CH4s
CH4	1	0	0	0	-1

Similarly, for the ECBM process the species in the system are: CH4 (g), CH4 (l), CO_2 (l), H2O (g), H2O (l), CH4(s), CO_2(s). The elements are: CH4, H2O and CO_2. The component-Element correlation matrix and reaction coefficient are tabled as table 4 and table 5

Table 4: Component-element correlation matrix

	CH4	H2O	CO_2	CH4(s)	CO_2(s)
CH4	1	0	0	1	0
H2O	0	1	0	0	0
CO_2	0	0	1	0	1

Table 5: Reaction coefficient matrix

	CH4(g)	H2O(g)	CO_2(g)	CH4(l)	H2O(l)	CO_2(l)	CH4(s)	CO_2(s)
CH4	1	0	0	0	0	0	-1	0
CO_2	0	0	1	0	0	0	0	-1

We can find that it is convenient for the simulator in modeling multi-component competitive sorption case. Results and validation are shown in the following section.

Results

Solutions to salt precipitation and pressure buildup during CO_2 injection into saline aquifers in Jianghan Basin

As discussed above, salt precipitation substantially reduces the reservoir permeability and severely causes pressure buildup around the injection well, which compromises the sustainable injection of CO_2. How to relieve the salt precipitation and pressure buildup is a technological problem faced when CO_2 is injected into the saline formations with high salinity. In this work, we tried to inject fresh water before injecting CO_2 to dilute the saline water. For base case, we first inject water for 2 months, and then inject CO_2 for 2 years. For reference case, we just inject CO_2 for 2 years.

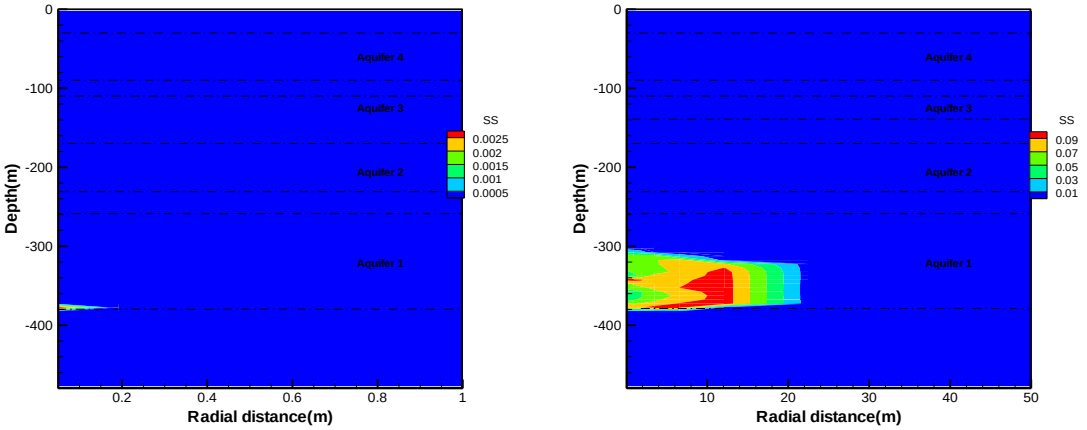

Figure 5: Solid saturation distribution of base case and reference case.

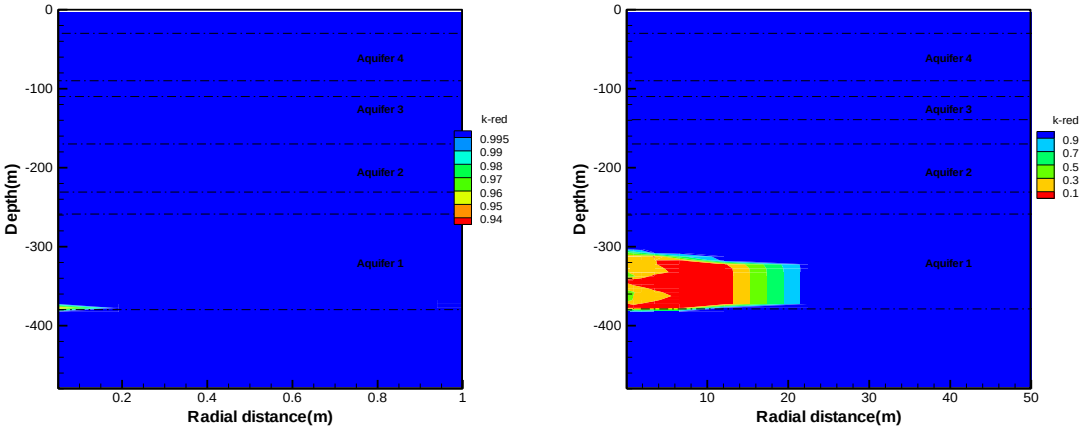

Figure 6: Permeability reduction distribution of base case and reference case

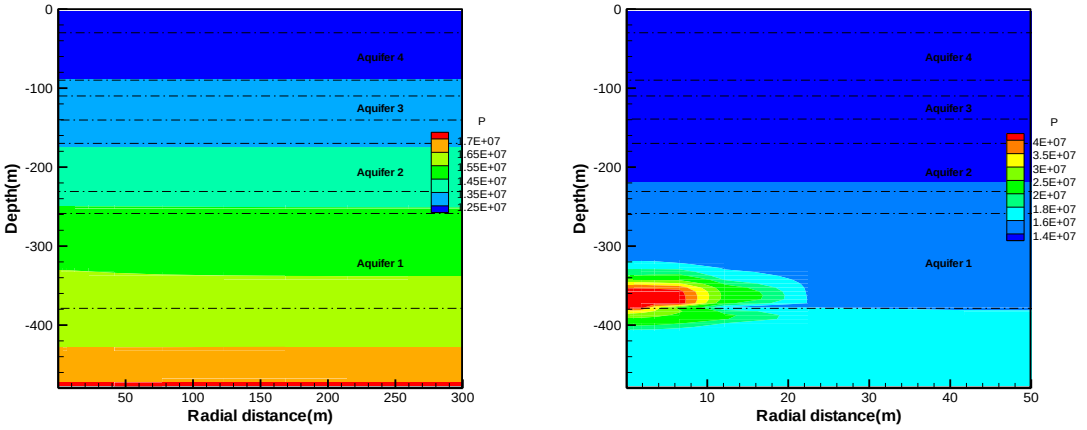

Figure 7: Fluid pressure distribution of base case

Figure 5, Figure 6 and Figure 7 present the distribution comparison of solid saturation, permeability reduction and fluid pressure of base case and reference case after 2years' CO_2 injection, respectively. There is a significant decline of salt precipitation by means of injecting fresh water to flush the saline formation before

CO_2 injection. The permeability of reservoir is near ly not influenced by the little salt precipitation. Therefore, there is no accumulation of fluid pressure around the injection well. For the reference case, the pressure around the injection well has reached 40Mpa.

Flushing the saline formation with the fresh water is an effective method to prevent the salt precipitation around the injection well when injection CO_2 into saline aquifers with high salinity. However, the fresh water is very precious, especially in the north China where water resource is very deficient. Taking into account the hydrochemical setting of saline aquifer of Jianghan Basin, we tried another way to relieve the salt precipitation and pressure buildup.

The brine resources in Jianghan Basin are in great abundance. The concentration of potassium ion is extremely high with the average value up to 1457.5 mg/L[25] in Qianjiang Depression. The brine resources have great potential for exploitation. The state and local government is planning to develop the potassium salt in large scale. Space will be made at the time of pumping water from the aquifers. In the present work, we tried to study the feasibility of injection CO_2 and pumping out saline formation water simultaneously to control pressure buildup while strong CO_2.The production well should be placed in a way that they should not interact with the injected CO_2 in order to avoid production of CO_2. It was achieved by placing the production well at 9.5km from theCO_2 injection well. It is assumed that the saline formation water can be extracted and processed at the industrial level in order to produce Commercial Salt.

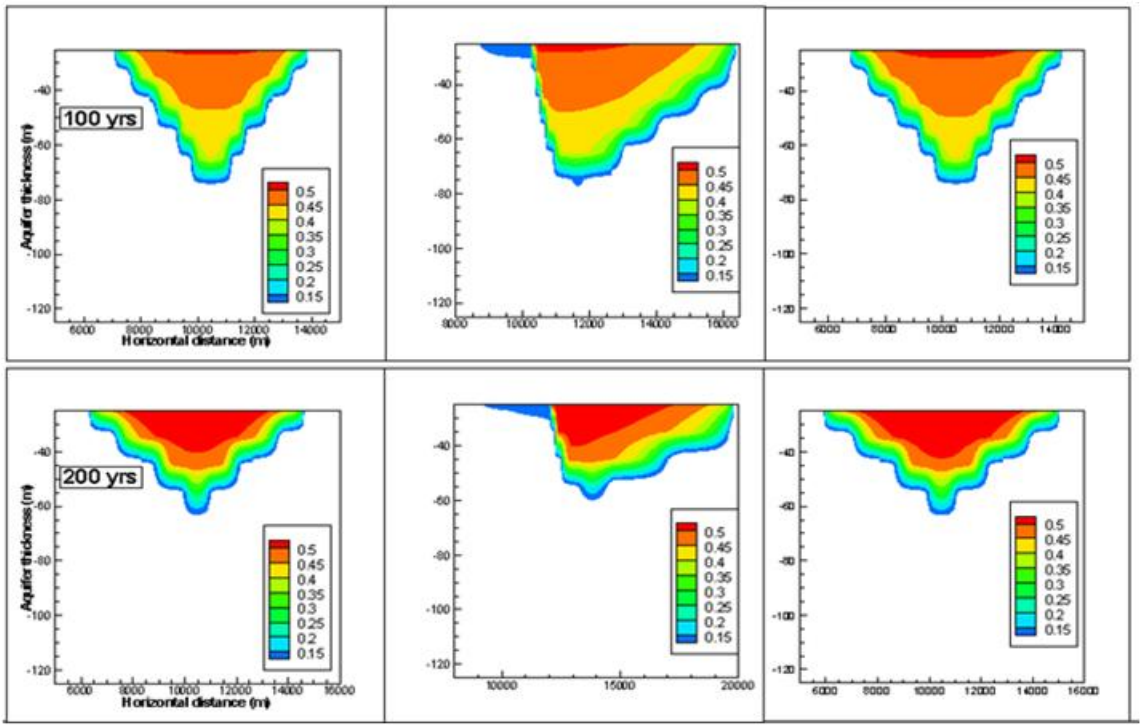

Figure 8: Distribution of CO_2 mobile phase for different times and for three cases of without (left plates), with (middle plates) one brine production well and with (right plates) two brine production wells.

Figure 8 shows the distribution of CO_2 mobile phase saturation for different times and for three cases without (left plates), with one production well (middle plates) and with two production wells, left side and right side of the injection well (right plates), the figure demonstrates that in case one production is used the CO_2 in gas phase will migrate towards the production well, on the other hand the introduction of the two wells (left side and right side of the production well) increases more or less the horizontal migration of the CO_2.

Solutions to salt precipitation and pressure buildup during CO_2 injection to saline aquifers in Jianghan Basin

Two methods were tried to relieve salt precipitation and pressure buildup during CO_2 injection. The method of pre-flush with fresh water before CO_2 injection can obviously alleviate the pressure buildup problem induced by halite precipitation around the injection well. In addition, this method could lower the salinity of the aquifers and increase the solubility of CO_2, with the benefit of reducing the leakage risk. Pumping saline water out of the target formation while injecting CO_2 simultaneously could reduce the pressure buildup both in the near-well region and the formation as whole. Increase in the saline water production rate leads to further decrease in pressure buildup, this phenomenon was demonstrated by tripling the production where the pressure decreased about 15 bars. The introduction of two wells (left side and right side of the production well) increases the horizontal migration of the CO_2 but contributes a little to the amount of CO_2 dissolved.

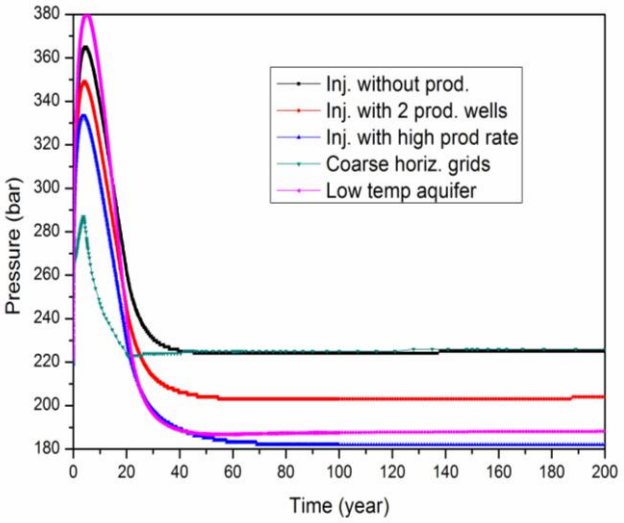

Figure 9: Baseline reservoir model with 20 years of injection, showing pressure evolution considering different parameters.

As is shown in Figure 9 the introduction of production wells decreases the maximum pressure buildup, even after the injection stops the pressure will be lower than the case of CO_2 injection without production wells. When the production was tripled (for each production well) the maximum pressure decreases further and it decreased about 15 bar lower than the base case. This shows that an increase in production rate leads to further decrease in pressure buildup and furthermore an increase in production rate will increase the brine quantity to be processed at the industry level in order to produce commercial salt.

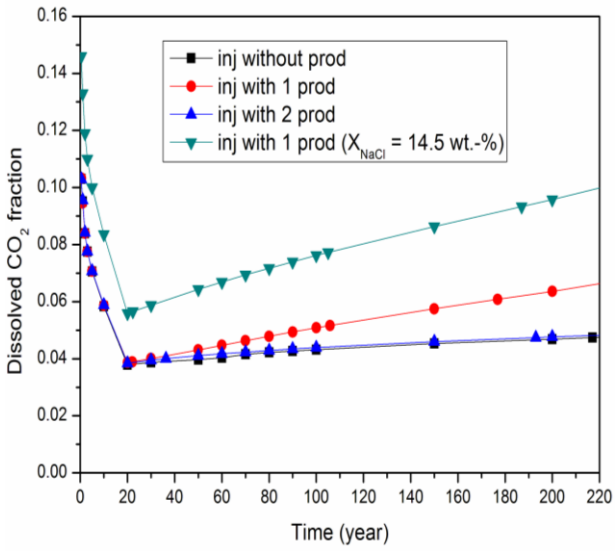

Figure 10: Comparison of CO_2 dissolved fractions in different cases.

Figure 10 demonstrates that CO_2 dissolution fraction depends on the salt mass fraction when the salinity became half of the base case mass fraction (14.5% instead

of 29%) the dissolved CO_2 fraction became higher and the same figure shows that the introduction of two injection wells (left and right sides of the injection well) contribute slightly to CO_2 dissolved amount, on the other hand when one side, although the introduction of one side production well induces the CO_2 mobile phase saturation to move toward the production well side but it also increases the CO_2 dissolved amounts.

Two gravity segregation experiments were performed with the apparatus. In the first experiment (experiment A) 90 cm3 of iC8 (~0.23 PV) was injected from the top of the column and in the second experiment (experiment B) 120 cm3 of iC8 (~0.31 PV) was used. Figure 11 reports the saturation distribution in the packed column as a function of time for the two segregation experiments. In experiment A, we observe that the non-wetting phase does not reach the top of the column after 24 hours. This indicates that the fluids in the column reach a gravity-capillary equilibrium before the plume reaches the top. To ensure that the plume reaches the top of the column, experiment B was performed with a larger initial volume (plume) of the non-wetting phase. From Figure 11 (right) we see that the plume in experiment B reaches the top of the column after approximately 24 hours and continues to migrate upwards at later times until the experiment was stopped after 72 hours.

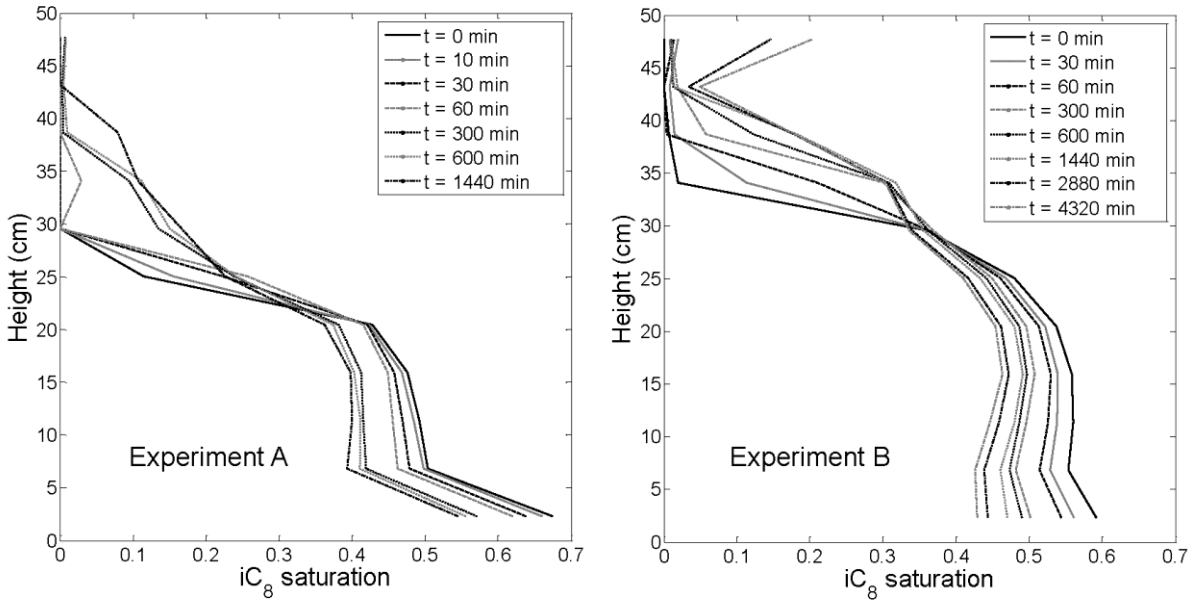

Figure 11: Saturation profiles of iC_8 in the column at various times; left: Experiment A and right experiment B

To simulate and interpret the experimental observations, we assume a 1D fluid flow and the physical properties of brine and iC8 (viscosity and density) are assumed to be constants. An IMPES formulation was used to solve the incompressible two-phase flow problem. In the numerical calculations we use a spatially refined model to reduce numerical diffusion and upscale (average) the calculation results to compare with the iC8 saturations from the experiments. The permeability is

assumed to be a constant (4.8 Darcy) in all cells, while the porosity in each cell of the refined model is set equal to the porosity of relevant section in the experimental setup. The initial iC8 saturation in the refined calculation is created from a piece-wise linear interpretation of the initial iC8 saturation in the experiment preserving the actual pore volume of the non-wetting phase.

Killough's model (Killough, 1976) was used to represent hysteresis in the relative permeability of both phases. Residual entrapment of iC8 was calculated from Land's model (Land, 1968) with Land's coefficient, C, obtained from the maximum residual non-wetting phase saturation observed in the steady-state relative permeability measurements. The scanning curves of the capillary pressure were obtained from Killough's model (Killough, 1976) by interpolation between the drainage and imbibitions curves.

From the measured and estimated input parameters, the changes in the wetting phase saturation in each section of the packed column are calculated in a purely predictive mode. The numerical calculations presented in this section are hence based on the co-current measurements and assume that there is no difference between co-current and counter-current saturation functions. Figure 12 compares the saturation profiles of iC8 as observed in the experiments with the calculated saturation profiles based on co-current model parameters.

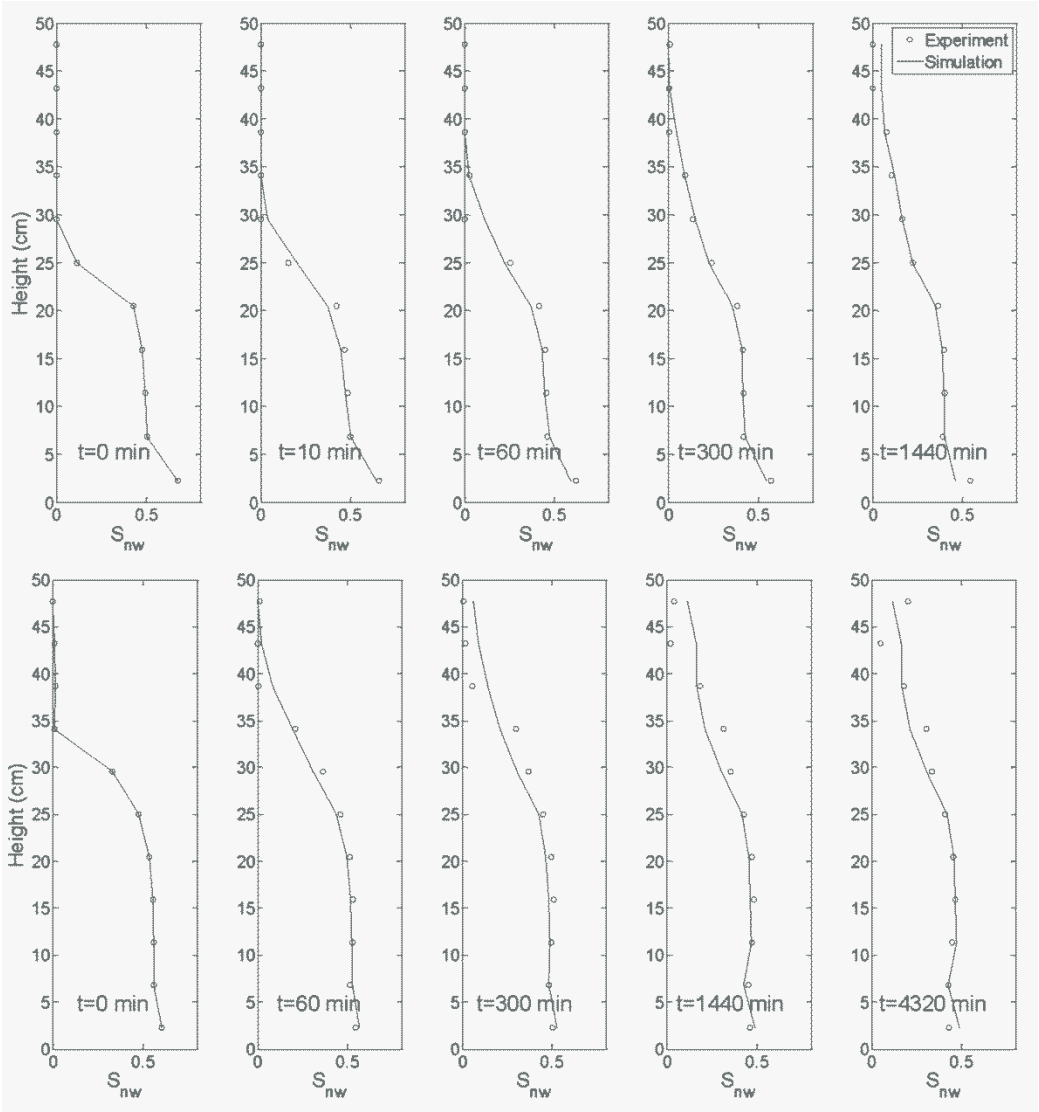

Figure 12: Saturation of iC8 in the column observed in the experiments and predicted based on co-current model parameters (upper panel: Experiment A, lower panel: Experiment B)

We observe that the iC8 plume is predicted to moves much faster by the numerical calculations than what is observed in the experiments. In the numerical calculation, the iC8 is predicted to reach the top of the column after only 5 hours for experiment A and after three hours in experiment B, while this is not observed in the experiment before after one day (24 hrs for experiment B). Therefore, we conclude that the numerical calculations based on co-current saturation functions fail to replicate the observed data. This is particularly evident for experiment B, where the arrival time of the plume at the top of the column is approaching an order of magnitude in error.

To match our experimental observations, model input parameters were changed by optimization. Lelievre (1966), Bentsen & Manai (1993) and Bourbiaux & Kalaydjian (1990) have demonstrated a reduction in the relative permeability functions for counter-current flow relative to co-current values. In the modification

of the model input parameters, two approaches were used to mimic counter-current relative permeability:

1) Fix the endpoint values of the relative permeability of both phases and adjust the saturation exponents – two adjustable parameters.

2) Adjust the endpoint relative permeability for the non-wetting phase, k_{re}, as well as the saturation exponent for both phases – three adjustable parameters.

From the first approach we found that the exponents of the relative permeability increase if the endpoint relative permeability of iC8 is kept constant and that the increase is more significant for iC8. In the second approach, the endpoint is decreased and the exponents of the relative permeability increase. The adjusted parameters from the second approach are consistent with previous studies where the endpoint relative permeability of the non-wetting phase is reduced during counter-current flow. If the iC8 endpoint relative permeability is kept constant, the saturation exponents increase further in the parameter estimation. In the second approach, the reduction of the relative permeability of the non-wetting phase during counter-current flow may be a consequence of factors beyond viscous drag: A new fluid configuration of the residual non-wetting phase can e.g. result in additional drag. Accordingly, the main contribution to the reduction in relative permeability cannot be isolated from the presented experiments and additional work is warranted on this topic. Figure 13 compares the numerical calculations with experimental observations after adjustment of model parameters (2nd approach) while Table 6summarizes the adjustment of the parameters used in the numerical calculations. The sum of relative errors is reduced significantly relative to the initial input by any of the approaches used in matching the experimental observations.

The difference between measured and adjusted relative permeabilities clearly demonstrates that the relative permeability measured in a co-current flow regime cannot be used to accurately predict the dynamics in a counter-current flow regime.

Table 6: Comparison of observed and adjusted input parameters

Experiments\Parameters	n_w	n_{iC8}	$k_{re,nw}$	*Error*
Co-current	3.8	1.7	0.15	25.4
Adjustment (P1)	4.4	2.4	0.15	11.2
Adjustment (P2)	4.3	2.7	0.15	11.5
Adjustment (P3)	4.4	2.4	0.11	10.9

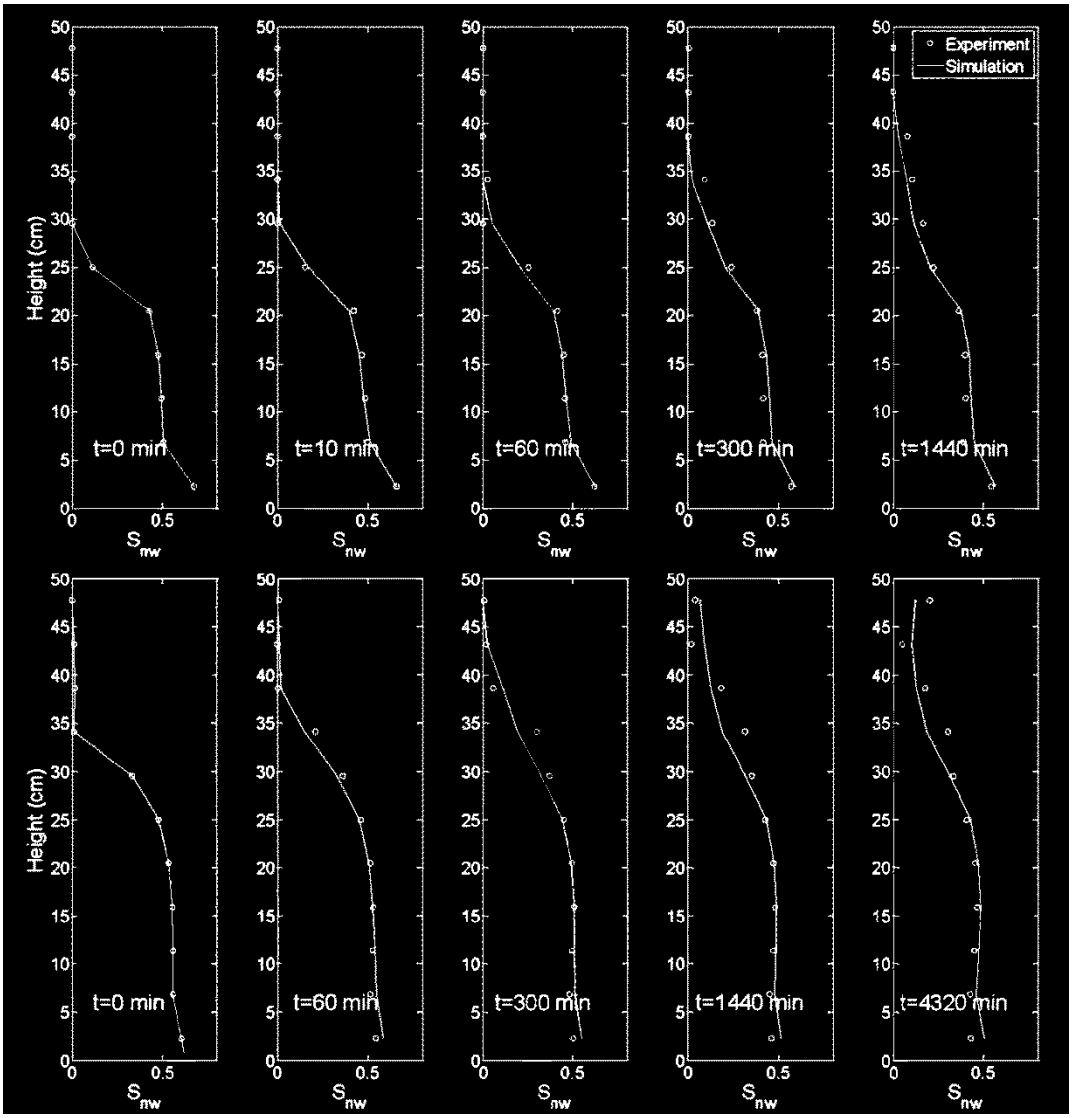

Figure 13: Comparison of experiments and simulation (A -upper panel, B- lower panel when endpoint non-wetting phase relative permeability is allowed to change (decrease).

Enhancement of Geochemical Simulator and the application of ECBM

Two methods of building ERA matrix are optimal in current GPRS. In this case the canonical matrix method is adapted. Canonical matrix for the reaction system mentioned above is expressed as:

0	-1	-1
-1	-1	-1
1	1	2
0	0	0
1	0	0
0	1	0
0	0	1

The corresponding ERA matrix is

1	0	0	0	0	1	1
0	1	0	0	1	1	1
0	0	1	0	-1	-1	-2
0	0	0	1	0	0	0

The extending ERA matrix needs a mineral part. It should be added according to the rule as former states. The validation is performed by comparing the molality of aqueous species H+ and Ca2+ after 10 days continuous injection. Results are shown in Figure 14 and 15. We can find that the GPRS can fit well with GEM.

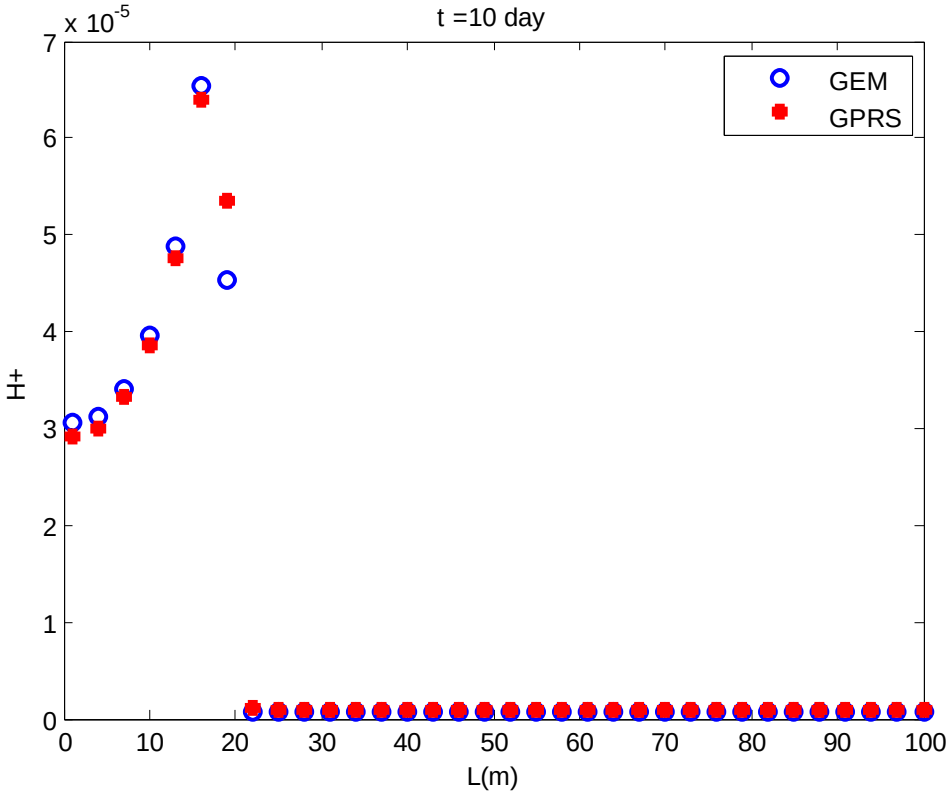

Figure 14: H+ molality distribution

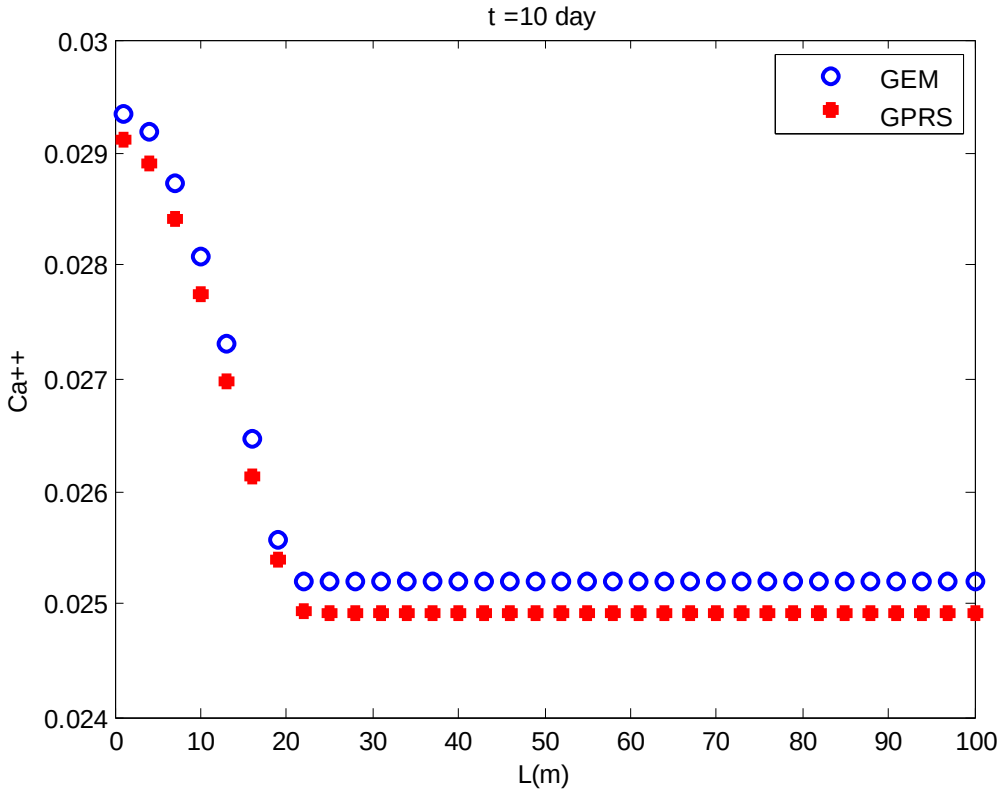

Figure 15: Ca2+ molality distribution

To validate the performance of the extended ECBM module, two cases are carried out. The first problem is dealing with CH4 depletion process. It is following the published work of Law et al. (2002). All the input data, such as Langmuir isotherm parameters, grid system, fracture relative permeability, well control are introduced. One difference is we assume the CBM reservoir is saturated with water initially. Eclipse300 and CMG-GEM simulator are participated in the comparison. The model we use in Eclipse300 is instant desorption single porosity model. GEM ECBM model is a dual porosity single permeability model. Both of them are pseudo compositional model and use Langmuir type sorption curve. Water component is not existed in the gas phase. Eclipse300 instant model requires a tiny desorption time, so we set 1e-3day for the input of both CMG-GEM and GPRS.

The first stage of production is water depletion. CBM reservoir pressure is decreasing as production continues. Meanwhile, gas desorption occurs due to pressure change. Peak production emerges at 10 days, and then decreases rapidly. Figure 16 shows the comparison of methane production rate for simulators. We can find that our results have good agreement with Eclipse300 and GEM. The deviation mainly comes from the initialization and model difference. Currently gas desorption hasn't been brought into the initialization part in GPRS, and the initialized adsorbed concentration in GPRS is set as an input parameter. It should be improved in the further work.

Case 2 is a CO_2 flooding process. The CBM reservoir model is the same as case

1. The desorption time for CH4 and CO_2 is 1 day. A constant injection rate of 7079.2m3/day is performed throughout the production period. The result that was shown in Figure 17 shows comparison of gas production rate for GEM and GPRS. In the former stage, the desorbed methane dominant the total gas production rate. The enhancement of methane production remains until CO_2 breakthrough occurs at the producer after about 60 days. In general, the gas production rate in the former stage fit well with GEM. A better fit can be derived through lower the initial adsorbed concentration to correct the difference in initialization. However our production rate is larger than the commercial software. A clear study shows the reabsorption model that GEM uses consider gas saturation, which hasn't been included in our model. A fine comparison is undertaken at present.

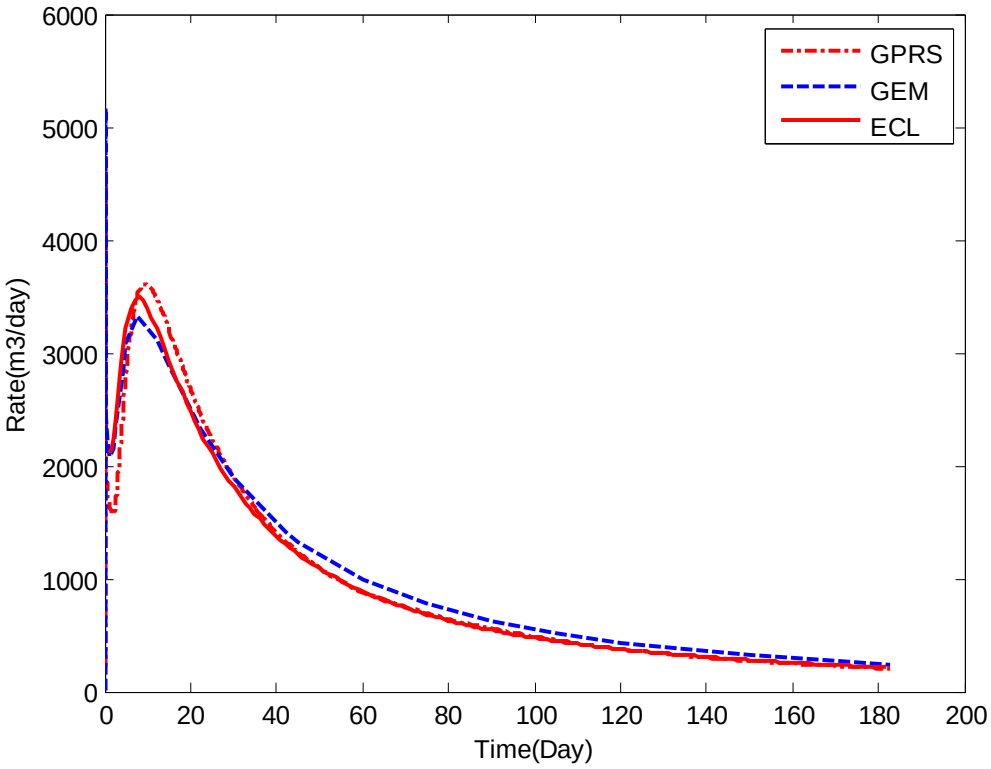

Figure 16: Gas production rate for primary recovery

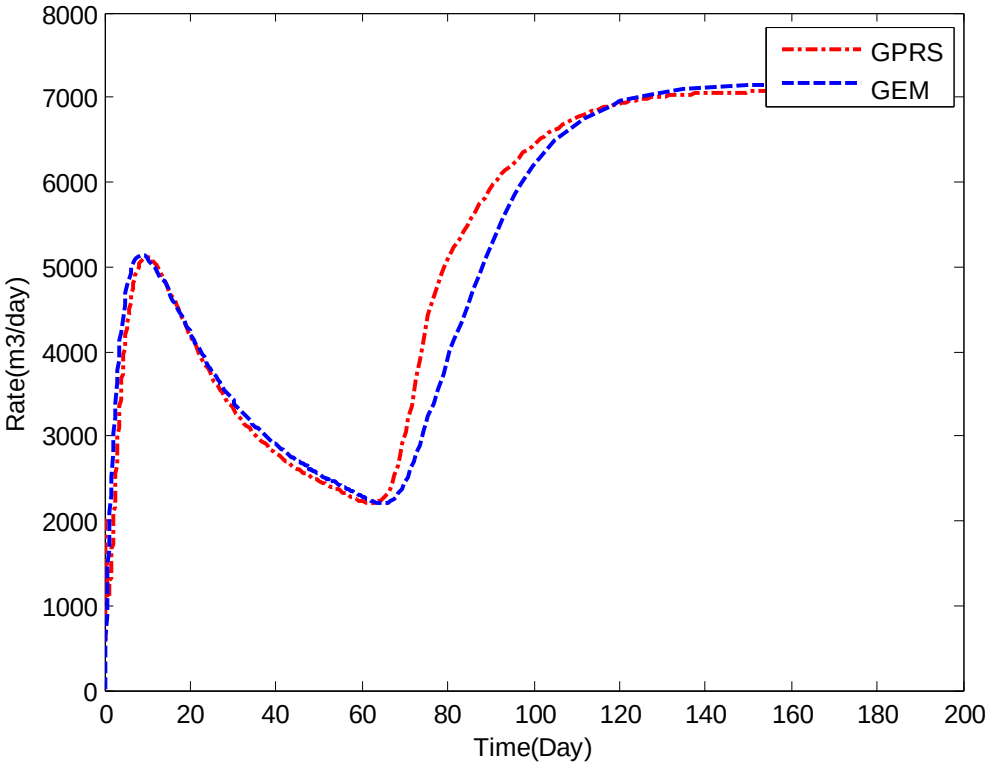

Figure 17: Gas production curve for CO_2 flooding

Progress

Solutions to salt precipitation and pressure buildup during CO_2 injection to saline aquifers in Jianghan Basin

Two methods were tried to relieve salt precipitation and pressure buildup during CO_2 injection. The method of pre-flush with fresh water before CO_2 injection can obviously alleviate the pressure buildup problem induced by halite precipitation around the injection well. In addition, this method could lower the salinity of the aquifers and increase the solubility of CO_2, with the benefit of reducing the leakage risk. Pumping saline water out of the target formation while injecting CO_2 simultaneously could reduce the pressure buildup both in the near-well region and the formation as whole. Increase in the saline water production rate leads to further decrease in pressure buildup, this phenomenon was demonstrated by tripling the production where the pressure decreased about 15 bars. The introduction of two wells (left side and right side of the production well) increases the horizontal migration of the CO_2 but contributes a little to the amount of CO_2 dissolved.

Dynamics of Plume Migration in Counter-Current Flows

Direct measurement of counter-current relative permeability is not trivial. In this study, we used an alternate approach to show that relative permeabilities that are

obtained in a co-current flow setting cannot be applied directly in the prediction of dynamics in counter-current flow settings. A comparison of measurements and predictions based on co-current observations show that the migration time of a non-wetting phase plume may be misrepresented by approximately an order of magnitude. Therefore, we propose that it is necessary to use a displacement dependent representation of relative permeability in the simulation of CO_2 injection into saline aquifers to represent the migration of CO_2 accurately.

Enhancement of Geochemical Simulator and the application in ECBM

To enhance the stability of GPRS geochemical simulator, a general scheme is designed. Two methods are employed to eliminate fast reaction rates in the aqueous phase. Element-component correlation matrix and canonical matrix are two strategies to build ERA matrix. Decomposing method is also investigated and applied. The fully coupled fully implicit simulator offers us a sufficient tool in modeling large scale and sophisticated CO_2 geological sequestration case.

The extended GPRS geochemical simulator has the ability of modeling ECBM process. Validations are performed by comparing the results with commercial software. The results show good agreements. It proves the feasibility of modeling Langmuir type reaction on the basis of GPRS platform. Reactions in the aqueous phase during ECBM can also be considered for an accurate simulation.

Future Plans

Further work considers addressing the following aspects. For the CO_2 injection and precipitation part, more factors are to be investigated and integrated for an optimal choice for CO_2 geological sequestration. To investigate the performance of dynamic relative permeability models, a fully implicit large scale simulation via GPRS is about to carry out. More work should be undertaken to enhance the performance of current GPRS chemical reaction simulator. The extended ECBM module will focus on the effect of high salinity in aqueous phase.

References

1. Bacci, G., A. Korre, S. Durucan (2011). Experimental investigation into salt precipitation during CO_2 injection in saline aquifers. Energy Procedia, 4:4450-4456, doi:10.1016/j.egypro.2011.02.399
2. Bacci, G., A. Korre, S. Durucan (2011). An experimental and numerical investigation into the impact of dissolution/precipitation mechanisms on CO_2 injectivity in the wellbore and far field regions. Int. J. Greenhouse Gas Control, 5, 579-588, doi:10.1016/j.ijggc.2011.05.007.

3. Pooladi-Darvish, M., S. Moghdam, D. Xu (2011). Multiwell injectivity for storage of CO_2 in aquifers. Energy Procedia, 4:4252-4259, doi:10.1016/j.egypro.2011.02.374.
4. APEC Energy Working Group EWG Project. CO_2 Storage Prospectivity of Selected Sedimentary Basins in the Region of China and South East Asia.2005
5. Li Guoyu, et al., 2002. Atlas of China's petroliferous basins [D]. Petroleum Industry Press.
6. DOE (2006) Carbon Sequestration Atlas of the United States and Canada: Appendix A - Methodology for Development of Carbon Sequestration Capacity Estimates [online]. National Energy Technology Laboratory, Available from: http://www.netl.doe.gov/publications/carbon_seq/atlas/Appendix%20A.pdf
7. CSLF (2005) Phase I Final Report: Task Force for Review and Identification of Standards for CO_2 Storage Capacity Measurement [online]. Carbon Sequestration Leadership Forum (CSLF) available from: http://www.cslforum.org/documents/PhaseIReportStorageCapacityMeasurementTaskForce.pdf.
8. CSLF (2007) Estimation of CO_2 Storage Capacity in Geological Media - Phase II [online]. Prepared by the Task Force on CO_2 Storage Capacity Estimation for the Technical Group (TG) of CSLF. available from: http://www.cslforum.org/documents/PhaseIIReportStorageCapacityMeasurementTaskForce.pdf.
9. Pan Guosi, Zhu Zhendong, 1988. The Symposium on structural features of oil gas bearing areas in China. The Petroleum Industry Press.
10. Yang Panxin, et al.2009, Structure Model and Evolution of the Jianghan Basin and Relation with Moderate to Strong Earthquakes [J], Earthquake, Vol.29, No.4, P123-131.
11. Jianghan Oilfield Company of China Petroeum. Petroleum Geology of Jianghan Oilfield [D]. Petroleum Industry Press.
12. Pruess, K., ECO_2N: A TOUGH2 Fluid Property Module for Mixtures of Water, NaCl, and CO_2. 2005, Lawrence Berkeley National Laboratory: Berkeley, CA.
13. Pruess K. and N. Spycher. ECO_2N – A Fluid Property Module for the TOUGH2 Code for Studies of CO_2 Storage in Saline Aquifers, Energy Conversion and Management, Vol. 48, No. 6, pp. 1761–1767, doi:10.1016/j.enconman.2007.01.016, 2007.
14. Narasimhan, T.N. and Witherspoon, P.A., An Integrated Finite Difference Method for Analyzing Fluid Flow in Porous Media. Water Resources Research, 1976. 12: p. 57-64.
15. Pruess, K., Oldenburg, C., and Moridis, G., TOUGH2 User's Guide, Version 2.0. 1999, Lawrence Berkeley National Laboratory: Berkeley, CA.
16. Chen Bo, Zhang ChangMin, Luo MingXia, Lei QingLiang, Han DingKun and Zhou XiaoJun, (2009)Hydrocarbon accumulation model of the Cretaceous in southern China, SCIENCE IN CHINA PRESS Springer, 52:77-87.
17. Xie Taijun, Wu Lizhen, Jiang Jigang, (1998) Oil and Gas fields in the Jianghan Basin, Hubei Province, China, Wagner H C Wagner, L C , Wang F F H and Wong, F.L., editors, 1988, Petroleum resources of China and related subjects: Houston, Texas, Circum-Pacific Council for Energy and Mineral Resources Earth Sciences Series, 10: 345-358.
18. Li, X., Wei, N., Liu, Y., Fang, Z., Dahowski, T.R., Davidson, L.C, (2009). CO_2 point emission and geological storage capacity in China. Energy Procedia, 1.2793-2800.
19. Pruess, K. Formation dry-out from CO_2 injection into saline aquifers: Part 1, Effects of solids precipitation and their mitigation. 2009. Lawrence Berkeley National Laboratory: Lawrence

Berkeley National Laboratory. LBNL Paper LBNL-1584E. Retrieved from: http://escholarship.org/uc/item/9p44q7x3

20. Zeidouni, M., Pooladi-Darvish, M., and Keith, D. Analytical Solution to Evaluate Salt Precipitation during CO_2 Injection in Saline Aquifers. Energy Procedia, 2009. 1(1): p. 1775-1782.
21. Garcia, E. Fluid dynamics and carbon dioxide disposal into saline aquifers. PhD thesis. 2003. University of California, Berkeley, USA.
22. Verma, A., Pruess, K. Thermohydrological conditions and silica distribution near high-level nuclear wastes emplaced in saturated geological formations. Journal of Geophysical Research, 1988. 93(B2). 1159-1173
23. Han, SW., McPherson, B. Comparison of two different equations of state for application of carbon dioxide sequestration. Advances in Water Resources, 2008. 31. 877-890.
24. Battistelli, A., Calore C., and Pruess, K. The Simulator TOUGH2/EWASG for Modeling Geothermal Reservoirs with Brines and Non-Condensible Gas. Geothermics, 1997. Vol. 26, No. 4, pp. 437 - 464.
25. Yu, S.S.,1994. The hydrochemical characteristics of hte deep brines in Jiangban Basin, Hubei. Journal of Salt Lake Science, 2(1):6-17.
26. Bentsen, R., & Manai, A. (1993). On the use of conventional cocurrent and countercurrent effective permeabilities to estimate the four generalized permeability coefficients which arise in coupled, two-phase flow. Transport in Porous Media , 11 (3), 243-262.
27. Bourbiaux, B., & Kalaydjian, F. (1990). Experimental study of cocurrent and countercurrent flows in natural porous media. SPE Reservoir Engineering, 5 (3), 361-368.
28. Cinar, Y., Jessen, K., Berenblyum, R., Juanes, R., & Orr Jr., F. (2006). An experimental and numerical investigation of crossflow effects in two-phase displacements. SPE Journal , 11 (2), 216-226.
29. Dawe, R., Wheat, M., & Bidner, M. (1992). Experimental investigation of capillary pressure effects on immiscible displacement in lensed and layered porous media. Transport in Porous Media , 7 (1), 83-101.
30. Killough, J. (1976). Reservoir simulation with history-dependent saturation functions. SPE Journal , 16 (1), 37-48.
31. Land, C. (1968). Calculation of imbibition relative permeability for two- and three-phase flow from rock properties. SPE Journal , 8 (2), 149-156.
32. Lelievre, R. (1966). Etude d'ecoulements diphasiques a contre-courant an en miliew poreux, comparaison avec Les ecoulements de meme sens. University of Toulouse, France: Ph.D Dissertation.
33. Leverett, M. (1941). Capillary behaviour in porous solids. Transactions of the AIME , 142, 152–169.
34. van Genuchten, M. T. (1980). A closed-form equation for predicting the hydraulic conductivity of unsaturated soils. Soil Science Society of America Journal , 44 (5), 828-928.
35. Law, D.H. -S., van der Meer, L.G.H., and Gunter, W.D. 2002. Numerical Simulator Comparison Study for Enhanced Coal Bed Methane Recovery Process, Part I: Pure Carbon Dioxide Injection. Paper SPE75669 presented at SPE Gas Technology Symposium, Calgary, Alberta, Canada, April 30-May 2. doi: 10.2118/75669-MS
36. GEM version 2009 User's Guide, Computer Modeling Group Ltd., 2009
37. Eclipse Version 2012 Technical Description, Schlumberger, 2010.

Contacts:

Dongxiao Zhang	donzhang@usc.edu
Kristian Jessen	jessen@usc.edu
Hamid Jahangiri	hjahangi@usc.edu
Dalad Nattwongasem	nattwong@usc.edu
Bin Gong	gongbin@coe.pku.edu.cn
Qingdong Cai	caiqd@mech.pku.edu.cn
Haibin Chang	hb-chang@163.com
Yi Zheng	yizheng@coe.pku.edu.cn
Xuan Liu	occultliu@gmail.com
Zhijie Wei	wjzweizhijie@126.com
Xiang Li	yesyou@pku.edu.cn
Yongbin Zhang	zybpkucoe@gmail.com
Yilian Li	yl.li@cug.edu.cn
Yanxin Wang	yx.wang@cug.edu.cn
Jianmei Cheng	jmcheng@cug.edu.cn
Wei Zhang	zhangwei_cug@qq.com
Ling Jiang	jiangling84yy@gmail.com
Gengbiao Qiu	276450108@qq.com
Qi Fang	frances2009@foxmail.com
Yibing Ke	ke.yibing.kevin@hotmail.com
Peng Cheng	042041cheng@163.com
Sanxi Peng	heiyingpsxq@163.com
Ronghua Wu	wuronghua050@163.com
Kabera Telesphore	kaberacris@yahoo.fr
Anne Nyatichi Omambia	tichiomambia@gmail.com
Jianxiong Dong	dong12205206@163.com